INFLUENCE OF A SMALL INLET IN A LARGE BAY

A.J. Mehta and T.A. Zeh

Department of Coastal and Oceanographic Engineering,
University of Florida, Gainesville, Florida 32611 (U.S.A.)

ABSTRACT

The tidal influence of a small inlet in a large, shallow bay has been investigated. The inlet, Sikes Cut, connects the Gulf of Mexico to Apalachicola Bay, which is a major oyster producing and, therefore, economically important coastal body of water in Florida. The role of the inlet is believed to be to facilitate the introduction of oyster predators from the Gulf into the bay, where some of the oyster reefs have been degrading in recent years, a matter of concern to the oyster industry. The flood and the ebb flow distributions near the inlet have been described, given certain assumptions concerning the flow regime, and these distributions have been verified by measurements. The predicted flow distributions under spring tidal conditions indicate that Sikes Cut has a relatively small influence in the bay, and that other explanations must be sought as causative factors for reef degradation.

INTRODUCTION

When a large bay is connected to the sea by multiple tidal inlets, the influence of any particular inlet on the tidal motion in the bay, especially if this inlet is smaller than the others, is generally localized to the bay region immediately surrounding the inlet. Nevertheless in some situations, the extent of this localized influence is a matter of environmental and economic concern. Fig. 1 shows Sikes Cut, a small man-made inlet which connects the Gulf of Mexico to Apalachicola Bay in Florida's panhandle. This comparatively large and shallow bay produces nearly ninety percent of oysters in Florida and is, therefore, of considerable importance to the oyster industry. The bay is approximately 20 km long and 10 km wide, and is connected to the Gulf through St. Vincent Sound, West

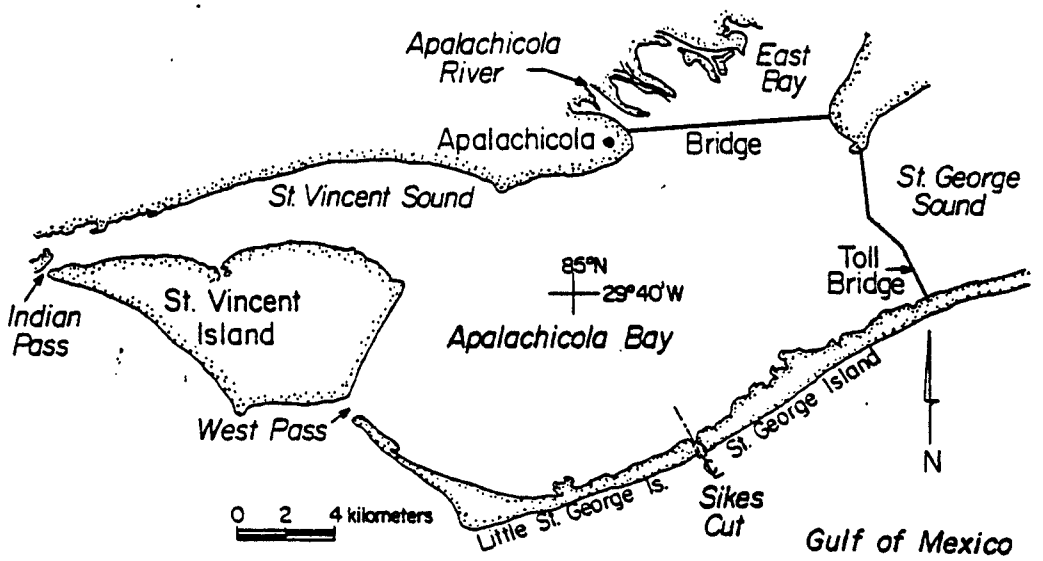

Fig. 1 Study Site

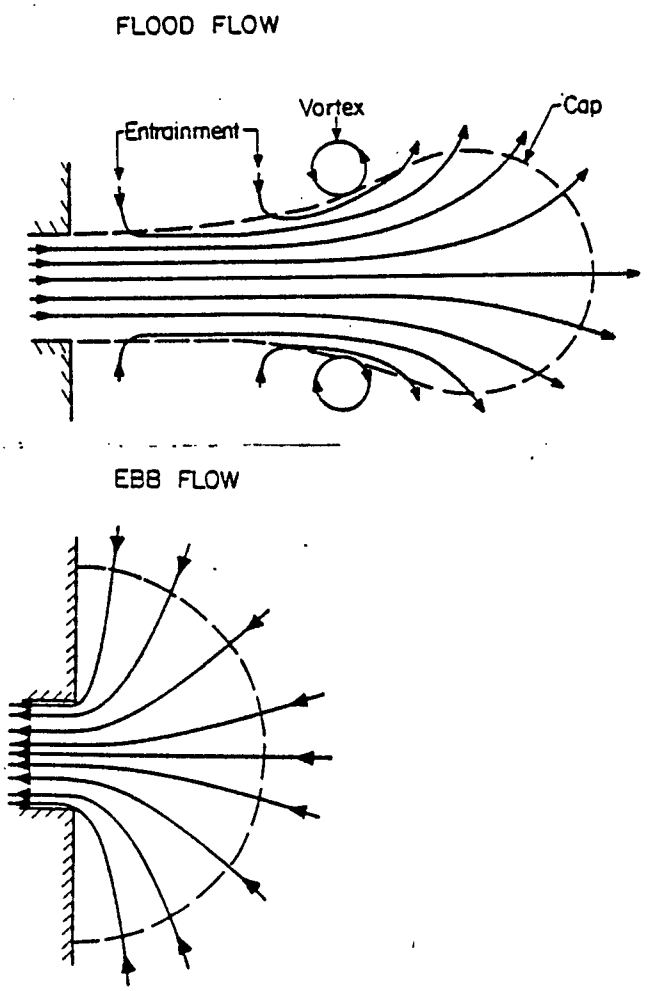

Fig. 2 A Simplified Jet-Sink Description of Flow near an Inlet

Pass, Sikes Cut and St.George Sound. Apalachicola River, a supplier of fresh water, enters the bay through East Bay near the town of Apalachicola. Sikes Cut was dredged in 1954 across St. George Island, which is a narrow barrier island, in order to facilitate the movement of shrimp trawlers between Apalachicola and the Gulf. Some of the oyster reefs in the vicinity of the inlet have been degrading in recent times, and the concern was that the degradation is due to the presence of Sikes Cut. Essentially, the role of this inlet is to introduce Gulf waters into the bay, and to apparently bring along with these waters such oyster predators as the Southern Oyster Drill and Crown Conch, which damage the reefs. The objective of this study was therefore to investigate the distribution of the tidal flow in the bay near Sikes Cut. The results of the investigation have been interpreted in terms of the extent of influence of the inlet in bay waters, and possible consequences, if any, to the existing oyster reefs.

DESCRIPTION OF THE FLOW PATTERN

Of interest in this study is the pattern of the flow in the bay issuing from the inlet during flood as well as entering the inlet during ebb. The flood flow distribution is considered as a non-buoyant turbulent jet, whereas the ebb flow is represented approximately in terms of the inlet as a flow sink, as illustrated in a simplified manner in Fig. 2. Following low water slack, the flood jet issues initially as a source flow which gradually separates from the boundaries. This separation induces vortices as shown, and later, a plume develops in the near-field of the inlet, while the vortices and the frontal cap of the jet continue to advance (Özsoy, 1977). Along the jet boundaries, flow is entrained from the ambient waters, thus enhancing its growth with distance. The advancement of the jet is arrested when the water level in the bay approximately reaches high tide. At this time the penetration of the waters from the inlet reaches its fullest extent for a particular tidal range, a matter of interest in this study. Following this time, current reversal causes the flow to reenter the inlet during ebb in the manner of a sink flow. The boundaries of the ebb flow differ from those

of the jet so that the volume of water that enters the inlet has a different identity, at least partially, from the volume that issues from the inlet during flood. The sink flow continues until a time when the water level in the bay approximately reaches low tide. Such a pattern of flow near the inlet is modified if the waters are closely confined by the bay boundaries. If however, the bay is sufficiently large and unconfining as far as the inlet flow is concerned, as in the present case, the jet-sink description may be used to characterize the flow both seaward as well as bayward of the inlet. Under such a condition, and in the absence of strong wave action or fresh water outflow, the flow field is characterized by the bottom topography, the tidal range and a crossflow such as a longshore current on the seaward side, or a current normal to the inlet channel on the bayward side. The resultant field will typically have a more complex geometry than the one illustrated in Fig. 2 and may be skewed relative to the inlet centerline due to the effect of crossflow and the Coriolis acceleration.

FLOOD AND EBB FLOW DISTRIBUTIONS

Flood Flow

In describing the flow distributions, the flow will be assumed to be vertically well-mixed, i.e. any density stratification will be ignored. The modeling of flood flow as a turbulent jet was carried out by French (1960) and others who assumed the bottom to be of a constant depth with negligible flow resistance. The results thus obtained did not satisfactorily represent actual conditions. A more realistic modeling of non-buoyant inlet plumes was carried out by Özsoy (Özsoy, 1977; Ünlüata and Özsoy, 1977). His characterization incorporates the effects of lateral flow entrainment into the jet plume, variable bottom topography, bed resistance and crossflow. Özsoy compared his solutions to test results mainly from a small physical model in the absence of a crossflow and found a good agreement. In considering real inlets, Zeh (1979) has shown through an order of magnitude analysis that the Coriolis acceleration should, in general, be included in the governing

equations. The development of the jet equations, which has been extensively described by Özsoy (1977) and by Zeh (1979), is briefly summarized here.

Through an order of magnitude analysis it can be shown that, inasmuch as temporal changes are gradual over a tidal period, the characteristics of the plume trailing the frontal cap may be approximated by assuming steady state conditions. The cap itself is a transient feature, but in a jet which is well extended into the ambient waters close to time of high water, the inertia of the mass of water in the cap is reduced, and the cap itself typically occupies a small volume as compared to the volume of the plume. In this study, therefore, the "steady state" plume is given primary consideration. The cap is considered to be a part of the plume so that at least a portion of the cap volume is incorporated in the computations.

Fig. 3 is a definition sketch for the topography near the inlet which is specified in the cartesian x-y coordinate plane, with the x-axis along the inlet centerline. The characteristics of the plume itself are specified in the curvilinear x_*-y_* coordinates, with the x_*-axis along the plume centerline and the y_*-axis along the plume width. The width $2b(x_*)$ changes with distance from its initial value of $2b_o$ at the inlet of uniform depth h_o. There is a tendency for the plume to expand by lateral momentum exchange and flow entrainment along the boundaries, represented by a velocity $v_e(x_*)$. In the zone of flow establishment (Zfe), the middle core of width $2r_e(x_*)$ has a uniform velocity u_o, which is the velocity of the initial jet at the inlet. This core decreases in width until at $x_* = x_s$, $r_e = 0$. Beyond this point the zone of established flow (Zef) exists and the plume centerline velocity $u_c(x_*)$, which is equal to u_o at $x_* = x_s$, decreases with increasing x_*. At any given x_*, the velocity distribution in the jet is such that the velocity decreases from u_c at the centerline to $u_a\cos\theta$ at the boundary, where $u_a(x)$ is a gradually varying crossflow (negative downward), and θ is the polar coordinate as defined in Fig. 3. The deflection of the plume relative to

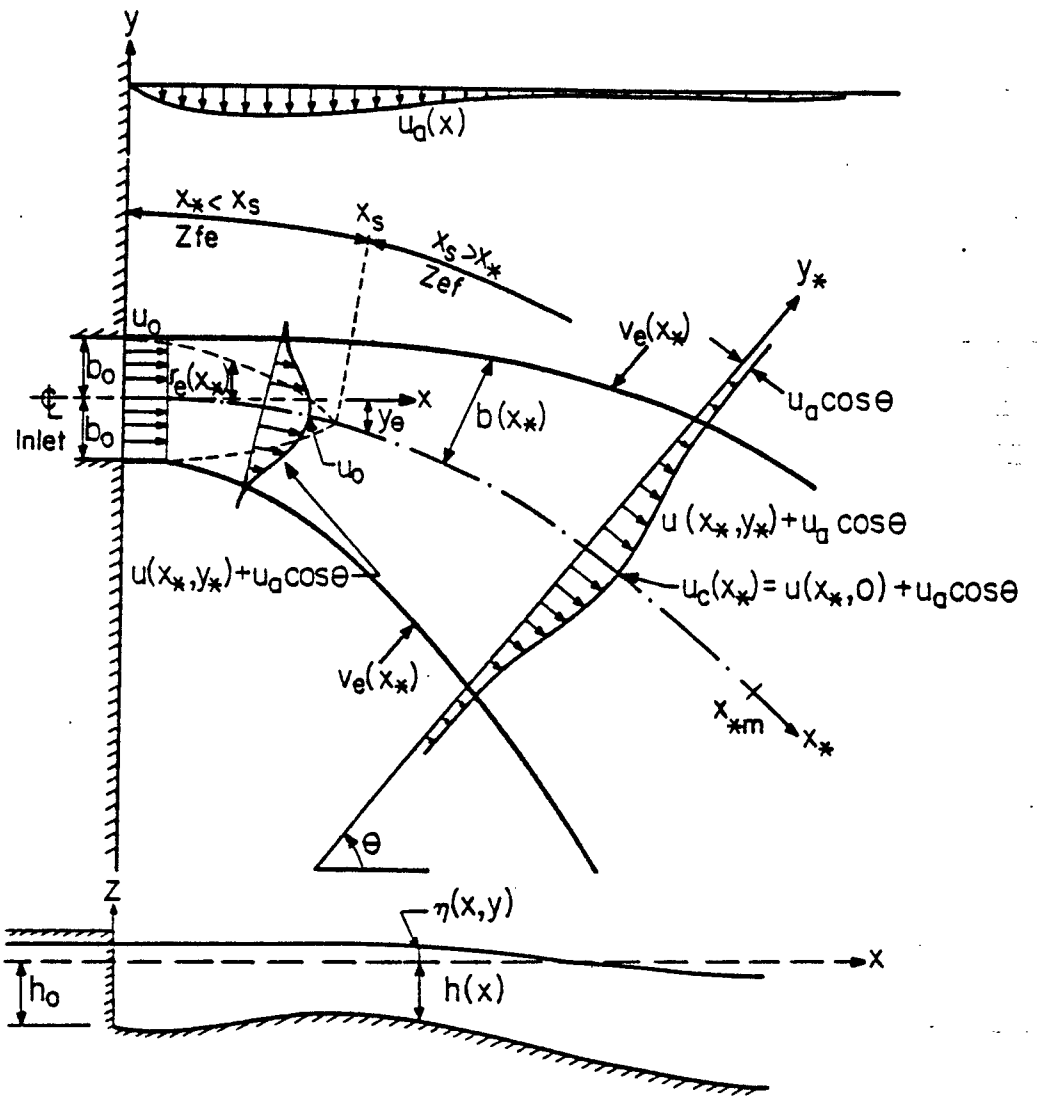

Fig. 3 Definition Sketch for Flood Plume

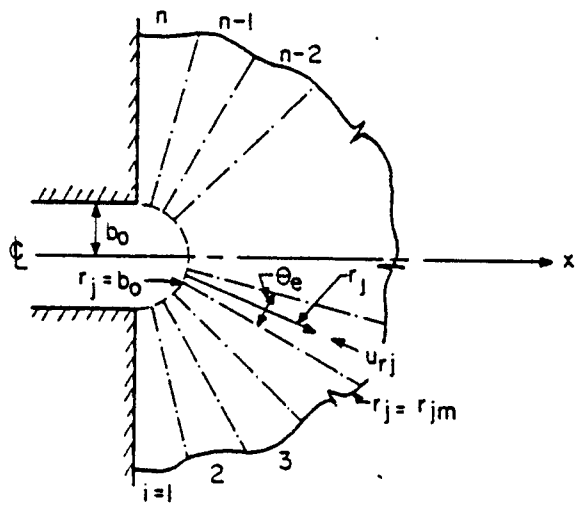

Fig. 4 Definition Sketch for Ebb Flow

the y = 0 axis (inlet centerline) is specified by y_θ. The three depth-averaged relationships, namely mass continuity and the two horizontal components of the momentum equation required to describe the plume are:

Mass continuity:

$$\frac{\partial}{\partial x_*}(hu) + \frac{\partial}{\partial y_*}(hv) = 0 \tag{1}$$

x-momentum:

$$\frac{\partial}{\partial x_*}(hu^2) + \frac{\partial}{\partial y_*}(huv) = -\frac{f}{8}u^2 - \frac{1}{\rho}\frac{\partial}{\partial y_*}(h\tau) \tag{2}$$

y-momentum:

$$\left(\frac{\partial\theta}{\partial x_*}\right) hu^2 = -gh\frac{\partial\eta}{\partial y_*} - 2hu\Omega\sin\phi \tag{3}$$

Here h(x) = depth of the bottom; u,v = time and depth-mean velocities along the x_*, y_* axes, respectively; $\tau = \rho\varepsilon\partial u/\partial y_*$ is the turbulent shear stress, ρ = water density, ε = eddy viscosity, f = Darcy-Weisbach friction factor; $\eta(x,y)$ = water surface displacement about h(x), Ω = earth's angular velocity and ϕ = latitude of the site. $\partial\theta/\partial x_*$ is the plume curvature and $(\partial\theta/\partial x_*)hu^2$ represents the centrifugal acceleration of the deflecting plume. Through an order of magnitude analysis, the centrifugal acceleration can be shown to be of the same order as the Coriolis acceleration which is represented by $2hu\Omega\sin\phi$. At Sikes Cut, the term $2\Omega\sin\phi$ = 0.000072 rad/sec. If the Coriolis acceleration and the crossflow are ignored, only Eqs. 1 and 2 are retained. If it is further assumed that the bottom depth is constant and that bed frictional resistance is negligible, Eqs. 1 and 2 reduce to forms which were analyzed classically by Albertson et al. (Daily and Harleman, 1966) in the laboratory and by French (1960) for inlets.

In order to integrate Eqs. 1, 2 and 3, certain assumptions with respect to the velocity field are necessary. These are 1) $v_e(x_*)$ is proportional to $u_c(x_*)$, i.e. $v_e = \alpha u_c$, where α = an entrainment coefficient; 2) $u_a(x)$ is not affected by entrainment, i.e. $v_e\sin\theta/u_a \ll 1$; 3) the crossflow is weak compared with the jet,

i.e. $u_a\cos\theta/u_c << 1$; and 4) the lateral velocity distribution in the plume as specified by $S = (u - u_a\cos\theta)/(u_c - u_a\cos\theta)$ is self-similar. This last assumption, which is also used in classical jet theory, relates the velocity distribution across the plume width at any given x_* to the centerline velocity, u_c. The incorporation of the self-similarity assumption facilitates the integration of the equations, and the specific function S selected is due to Stolzenbach and Harleman (1971), adapted by Özsoy (1977) to the problem of jet in a crossflow according to

$$S(y_*) = \begin{cases} 0 & ; \quad |y_*| > b \\ (1 - \zeta_o^{1.5})^2 & ; \quad r_e < |y_*| < b \\ 1 & ; \quad 0 < |y_*| < r_e \end{cases} \tag{4}$$

in the Zfe where $\zeta_o = (|y_*| - r_e)/(b - r_e)$, and

$$S(y_*) = \begin{cases} 0 & ; \quad |y_*| > b \\ (1 - \zeta^{1.5})^2 & ; \quad 0 < |y_*| < b \end{cases} \tag{5}$$

in the Zef where $\zeta = |y_*|/b$. Eqs. 1, 2 and 3 are next integrated across the plume width from $y_* = -b$ to $+b$, recognizing that the plume is symmetric about the $y_* = 0$ axis and utilizing the similarity functions of Eqs. 4 and 5 as well as the relationship $v_e = \alpha u_c$. Details are given by Özsoy (1977) elsewhere. The integrated equations are conveniently expressed in a dimensionless form by introducing the variables: $\xi = x_*/b_o$, $\psi = x/b_o$, $\chi = y/b_o$, $\mu = fb_o/8h_o$, $\tilde{h} = h/h_o$, $\tilde{b} = b/b_o$, $\tilde{u} = u_c/u_o$, $\tilde{u}_a = u_a/u_o$, $\tilde{r}_e = r_e/b_o$ and $\tilde{\Omega} = (2\Omega b_o/u_o)\sin\phi$. Thus Eq. 1 upon integration becomes

$$\frac{d}{d\xi}(\bar{I}_1 \tilde{h}\tilde{b}\tilde{u}) = \alpha\tilde{h}\tilde{u} \tag{6a}$$

where

$$\bar{I}_1 = \frac{\tilde{r}_e}{\tilde{b}} + [I_1 - (1 - I_1)\frac{\tilde{u}_a}{\tilde{u}}\cos\theta](1 - \frac{\tilde{r}_e}{\tilde{b}}) \tag{6b}$$

and

$$I_1 = \int_0^1 (1 - \zeta^{1.5})^2 d\zeta = 0.450 \tag{6c}$$

Eq. 2 becomes

$$\frac{d}{d\xi}\left(\bar{I}_2 \tilde{b}\,\tilde{u}^2\right) = \alpha \tilde{h}\,\tilde{u}_a \tilde{u}\cos\theta - \mu \bar{I}_2 \tilde{b}\,\tilde{u}^2 \tag{7a}$$

where

$$\bar{I}_2 = \frac{\tilde{r}_e}{\tilde{b}} + \left[I_2 - 2(I_1 - I_2)\frac{\tilde{u}_a}{\tilde{u}}\cos\theta + (1 - 2I_1 + I_2)\frac{\tilde{u}_a^2}{\tilde{u}^2}\cos^2\theta\right]\left(1 - \frac{\tilde{r}_e}{\tilde{b}}\right) \tag{7b}$$

and

$$I_2 = \int_0^1 (1 - \zeta^{1.5})^4 d\zeta = 0.316 \tag{7c}$$

When integrating Eq. 2, the shear gradient $\partial(h\tau)/\partial y_*$ vanishes by virtue of the assumption that the velocity gradient in the y_* direction is zero at the boundary, according to the functional form of the similarity function, since

$$\left.\frac{\partial S}{\partial y_*}\right|_{|y_*|=b} = \left.\frac{\partial u}{\partial y_*}\right|_{|y_*|=b} = 3\left[1 - \left(\frac{b}{b}\right)^{1.5}\right]\left(\frac{b}{b}\right)^{0.5} = 0 \tag{8}$$

Integration of Eq. 3 yields:

$$\bar{I}_2 \tilde{b}\,\tilde{u}\frac{d\theta}{d\xi} = -\alpha \tilde{u}_a \sin\theta - \tilde{\Omega}\,\tilde{b}\,\bar{I}_1 \tag{9}$$

Here, the integral of the pressure gradient term $-gh\partial\eta/\partial x_*$ was evaluated by the application of Bernoulli equation over the ambient entrainment flow field from $y_* = b$ to $y_* \to \infty$ (Özsoy, 1977). Two additional equations giving the relationship between the cartesian and the curvilinear coordinates arise. These are:

$$\frac{d\psi}{d\xi} = \sin\theta \tag{10}$$

$$\frac{d\chi}{d\xi} = \cos\theta \tag{11}$$

In the Zef, the core width $\tilde{r}_e = 0$ in Eqs. 6b and 7b. Eqs. 6, 7, 9, 10 and 11 form a set of ordinary differential equations with unknowns $\tilde{r}_e$, $\tilde{b}$, θ, ψ and χ in the Zfe and $\tilde{u}$, $\tilde{b}$, θ, ψ and χ in the Zef. These must in general be solved numerically, with appropriate initial conditions (in space) in the two zones. In the Zfe, the initial conditions specified at $\xi = \psi = 0$ are $\tilde{u}(0) = 1$, $\tilde{b}(0) = 1$, $\tilde{r}_e(0) = 1$,

$\theta(0) = \pi/4$ and $\chi(0) = 0$. In the Zef the initial conditions are specified at $\xi_s = x_s/b_o$ where $\tilde{u}(\xi_s) = 1$. The remaining conditions are obtained from the final values in the Zfe.

For computational purposes it was necessary to establish specific limits to the assumed inequalities, $v_e \sin\theta/u_a << 1$ and $u_a \cos\theta/u_c << 1$. From a practical standpoint, it was decided to select $v_e \sin\theta/u_a \leq 0.1$ and $u_a \cos\theta/u_c \leq 0.1$. Noting that the maximum value of $\theta = \pi/4$ occurs near the inlet, inserting this value in the first inequality gives $v_e/u_a \leq 0.1 u_a$ or $u_c/u_a \leq 0.1/\alpha$. Substituting this in the second inequality yields $\cos\theta \leq 0.01/\alpha$. As will be discussed later, an experimental value of $\alpha = 0.05$ in the Zef may be selected, thus giving $\theta \geq 78°$. The computed plume was allowed to deflect no more than this limit. Such a limitation also insures a reasonable validity of utilizing the similarity function for the plume velocity, as this function may be expected to describe the velocity field with some degree of accuracy only when the plume is deflecting gradually, and when the deflection itself is small, given a non-horizontal bottom. An approximation to the solution of the equations beyond the $\theta = 78°$ limit was obtained by setting Ω and u_a to zero. Such an approximation allows no further increase in the plume curvature, and yet permits an estimation of the maximum extent of the plume, which in reality may extend beyond the $\theta \geq 78°$ limit.

The set of equations together with the initial conditions and the θ limit were solved numerically using the Predictor Corrector Method (Hamming, 1968). The friction factor f was computed from

$$f = \frac{0.25}{[1.171 + \log(Hh_o/k_s)]^2} \qquad (12)$$

which is applicable in the fully rough range of flow, and where k_s = Nikuradse's equivalent sand roughness of the bed, which was estimated from measurements.

Extent of the Plume

An estimate of the longitudinal extent of the plume is obtained by equating

e volume P_j occupied by the plume to the sum of the tidal prism P_j through the inlet and the volume P_e entrained laterally through the plume boundaries during the flood. Accordingly,

$$P_j = P_t + P_e \tag{13}$$

ere

$$P_j = \int_{-h}^{\eta} \int_{-b}^{b} \int_{0}^{x_{*m}} dx_* dy_* dz \tag{14}$$

$$P_t = \int_{0}^{T_F} Q(t)dt \tag{15}$$

$$P_e \simeq 2T_F v_e \sum_{i=1}^{i=x_{*m}/\Delta x_*} h_i(x)(\Delta x_{*1}^2 + \Delta b_i^2) \tag{16}$$

re T_F = period of flood, $Q(t)$ = instantaneous discharge through the inlet and Δb_i = ith increment in the plume width for a corresponding increment Δx_{*i} along the plume centerline. q. 16 is an approximation which is reasonable only for a plume with gradually varying boundaries. I the above equations, x_{*m} is the longitudinal extent of the plume which satisfies Eq. 13 and must be obtained iteratively.

E b Flow

A description of the flow field while the flow is entering the inlet during ebb i found from mass continuity, incorporating the effect of a variable bottom topography in a approximate manner, but ignoring the effects of bed resistance and crossflow. Not considering these effects implies a somewhat restrictive treatment, but it may atleast be r cognized that typically, the radial extent of the ebb flow field is considerably less than the maximum penetration of the flood jet, and hence, the effects of bed resistance and c.ossflow are likely to be less significant in specifying the ebb flow field than flood.

The flow field is divided into n segments of equal angles θ_e as depicted in Fig. 4. At any radial position r_j, the depth h_j is considered to be constant in a given segment, t t is allowed to vary from segment to segment. The volume $\forall_j$ of the jth segment is given by

$$\forall_j = \theta_e \int_{-h_{mj}}^{\eta} \int_{0}^{r_{mj}} r dr dz \tag{17}$$

where θ_e is in radians, r_{mj} = the radial extent of the jth segment and h_{mj} = the depth at that distance. If the bottom were horizontal throughout, $\forall_j$ would be given by

$$\forall_j = \frac{P_t}{n} \tag{18}$$

In this case, all the segments have the same length $r_{mj} = r_m$; thus Eq. 17 becomes

$$\frac{P_t}{n} = \frac{\theta_e h r_m^2}{2} \tag{19}$$

Eq. 19 was used by Taylor and Dean (1974) to solve for r_m, given P_t. For the general case in which h_{mj} is variable, it is assumed in this analysis that $\forall_j$ is proportional to the flow area $A_{mj} = \theta_e r_{mj} h_{mj}$, at the farthest boundary of the jth section; hence

$$\forall_j = \frac{A_{mj}}{\sum_{i=1}^{i=n} A_{mi}} P_t \tag{20}$$

Given T_E=ebb period, P_t/T_E is the mean discharge during ebb and $\forall_j/T_E$ is the mean discharge through the jth segment. The factor $A_{mj}/\sum_{i=1}^{i=n} A_{mi}$ thus is a weighting factor fo the discharge through the jth segment. Given segments of equal angle θ_e, the weighting is according to the depth h_{mj} at the boundary of the jth segment, a small depth giving a low discharge and so on. In Eqs. 17 and 20, the two unknowns are $\forall_j$ and r_{mj}, noting that for a given r_{mj}, the summation $\sum_{i=1}^{i=n} A_{mi}$ can be derived from the topography. These two equations must be solved iteratively, with an initial approximation of $\forall_j$ obtained from Eq. 18. Within the boundaries $r_j=b_o$ and $r_j=r_{jm}$, the flow velocity $u_{rj}(t)$ is then obtained from

$$u_{rj}(t) = \frac{2\pi \forall_j}{T_E \theta_e h_j r_j} \sin(\frac{4\pi}{T_E} t) \tag{21}$$

where a simple harmonic variation of the flow with time is assumed.

FIELD PARAMETERS

Hydraulic measurements were made near the inlet in August, 1978. In addition, an aerial photograph of the inlet taken in May 1978, showning a plume in the bay was used in corroborating the results. The bottom topography of the region in August, 1978, is shown in Figure 5. Shoaling of the inlet occurs due to sediment

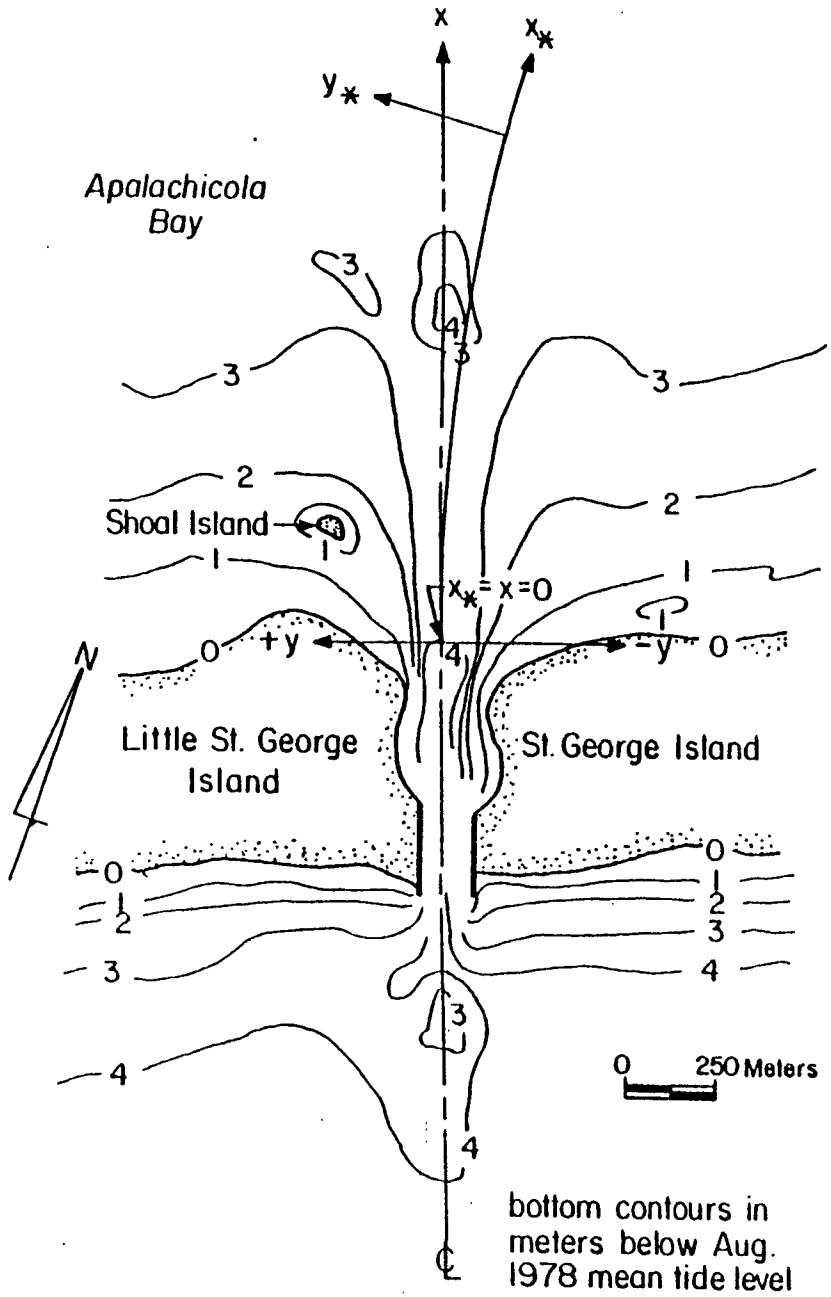

Fig. 5 Bottom Topography near the Inlet

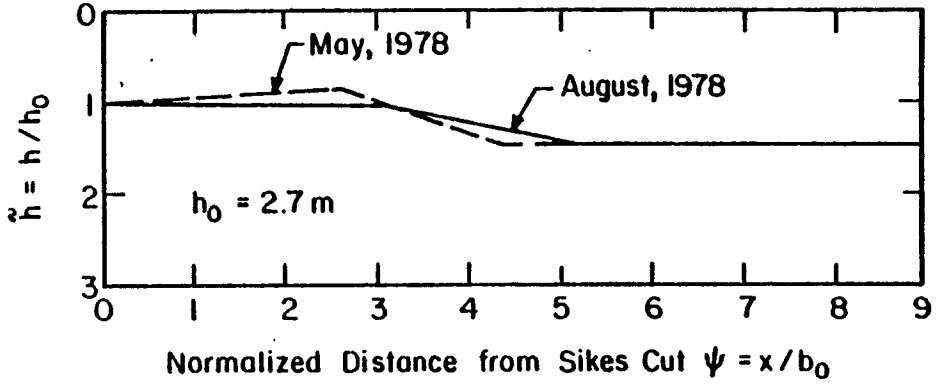

Fig. 6 Idealized Bottom Topography near the Inlet

Fig. 7 Incipient Flood Plume, May 1978

input from the Gulf, and a 60 m wide and 3-4 m deep channel is maintained by annual dredging. The bottom sediment consists primarily of quartz sand with a median diameter of 0.24 mm. A notable feature is the shoal island due to dredge spoil deposition in June, 1978 on the western bay side of the inlet channel. The topography is comparatively complex and does not conform to the assumption of parallel depth contours. Furthermore, the shoal island clearly poses a problem for geometric simplification. Nonetheless, if 1) an x=0 line is defined such that the volumetric defect of land on the bayward side of this line caused by the 0 m (mean tide level) contour is balanced by the corresponding volumetric protrusions of the land and 2) a weighting is given to the shoal island, then the average topography shown in Fig. 6 results. The half-width b_o and depth h_o are defined at the cross-section where the x=0 line intersects the inlet, as shown in Fig. 5. Fig. 6 also shows the May, 1978, topography, which differs from the August topography as a result of inlet dredging and spoil deposition in June. The topographies of Fig. 6 were utilized in the computations, bearing in mind the limitations imposed by the approximations to the actual bottom variation.

The tide was semi-diurnal with a range of 0.32 m on the bayward side. Salinity profiles indicated a vertically mixed flow regime (Zeh, 1979). This mixing is attributed to the tidal energy, low fresh water outflow and wind wave-induced turbulence near the surface. Waves on the order of 0.5 m were present. Some salinity measurements obtained at another time under a similar freshwater flow from the Apalachicola River, a higher tidal range (0.50 m) but less than 0.2 m waves indicated a significant degree of density stratification, thus suggesting that wind waves play a very important role in producing a mixed flow strucutre in this region.

The flood plume, as it entered the bay and extended, was clearly visible because of the slightly more turbid waters within the plume as compared with the bay waters, with a clear demarkation of the boundaries. The plume deflected

eastward of the inlet centerline as marked in Fig. 5. Currents were measured at several positions in the inlet and in the bay near the inlet during flood and later, at spring tide, at a few positions during an ebb flow. Plume width was marked by noting the visual position of the boundary, with reference to floating markers. A view of the inlet showing an incipient plume in May, 1978, is shown in Fig. 7. Note may be made of the visual distinction between the plume and the ambient waters.

The currents were used to estimate 1) the bed roughness k_s and 2) the entrainment coefficient α. k_s was derived from Manning's equation, and a representative average of 0.031 m was estimated for the plume region. This gives a roughness-grain size ratio of 0.031/0.00024 = 129, indicating the presence of ripples or dunes at the bed. In the inlet itself, k_s = 0.29 m was estimated.

The entrainment coefficient α has different magnitudes in the Zfe (α_1) and Zef (α_2), with α_2 being less important of the two inasmuch as Zfe is typically small compared to Zef in inlets. An estimate of α_2 based on measurements is given in Table 1. The coordinates of the two stations, both of which were outside the plume, are referenced to the plume centerline. According to the data given, at an average longitudinal distance ξ = 5.8, v_e = 0.070 m/sec, u_c = 0.340 m/sec and u_a = 0.01 m/sec in the westerly direction. Thus $\alpha_2 = v_e/u_c$ = 0.21, which is considerably higher than α_1 = 0.036 and α_2 = 0.050 evaluated from laboratory measurements (Özsoy, 1977).

TABLE 1

Calculation of Entrainment Coefficient, α_2

Station	Coordinates		Entrainment Velocity, v_e in m/sec	Plume Waterline Velocity, u_c in m/sec
	ξ	ζ		
West of Centerline	5.3	1.3	0.080	0.340
East of Centerline	6.2	-1.5	-0.060	--

RESULTS

Computations were initially carried out with a $\alpha_1 = 0.036$ and $\alpha_2 = 0.21$, but it was found that this value of α_2 gave excessive entrainment; as a result $\alpha_2 = 0.05$ selected and was found to be reasonable. A likely explanation for the large measured value of α_2 is that the data of Table 1 corresponded to a time when the frontal cap had just moved past the $\xi = 5.8$ position. The plume at this position was therefore in a transient stage, and was entraining flow at a higher rate than permitted according to the steady state assumption.

Fig. 8 shows the variation of the inlet velocity u_o with time t. The data are normalized so that $\nu = u_o/(gR_I)^{\frac{1}{2}}$, where R_I is the tidal range at the inlet and $\theta_t = t/T$, where T = tidal period. In Fig. 9, the plume centerline velocity is presented. The position of the centerline was determined from the plume boundaries; the centerline at each distance from the inlet being considered approximately as the halfway point between the boundaries. Since the position of a measuring station did not necessarily coincide with the plume cneterline, the similarity function of Eq. 5 was used to obtain $u_c(x_*)$ from the measured $u(x_*, y_*)$, given $u_a = 0.01$ m/sec. The data points at $\xi = 5.3$ and 9.2 were derived in this manner. The validity of the similarity function is attested to a degree by the comparison between measurement and Eq. 5 in the inset of Fig. 9. This lateral velocity distribution was obtained at $\xi = 5.8$. Returning to the centerline velocity, a decreasing trend in the Zef is exhibited both by the data and by the solution of the equations although the data show slightly higher values of u_c. This distribution was obtained at $\theta_t = 0.82$, with $u_o = 0.76$ m/sec derived from Fig. 8. In the computations, the position of the instantaneous water surface level at any θ_t with reference to the mean tide level was accounted for in specifying the bottom topography. Computations probably exagerate the length of the Zfe, since in reality the lateral velocity distribution in the inlet was not uniform as assumed, but was close to parabolic. Such an initial condition has the effect of reducing the core length in comparison with what is predicted by assuming a uniform distribution.

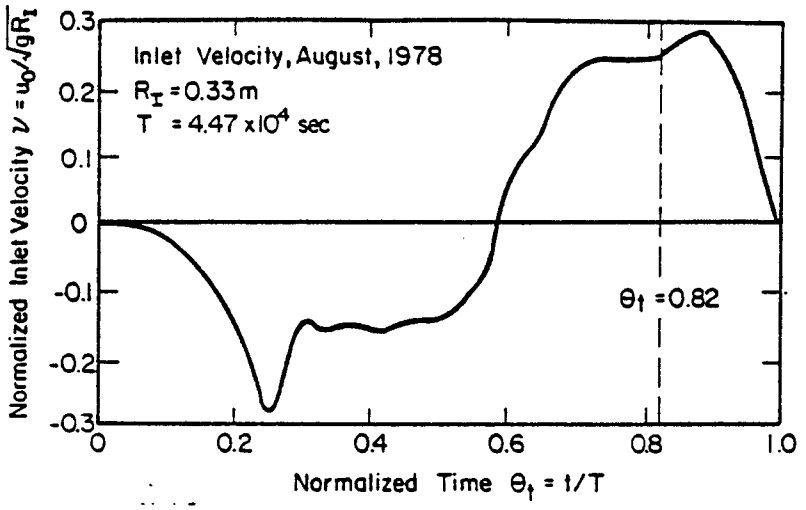

Fig. 8 Inlet Velocity, August 1978

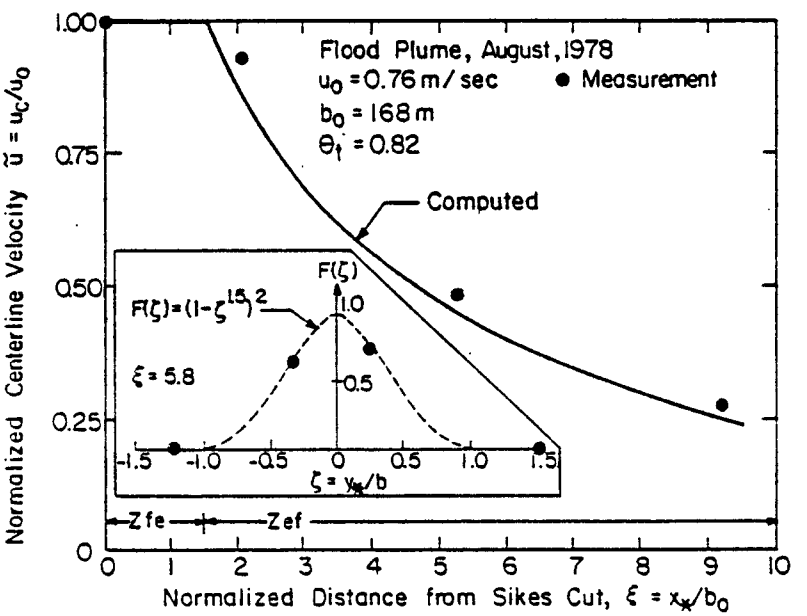

Fig. 9 Flood Plume Centerline Velocity and Lateral Velocity Distributions, August 1978

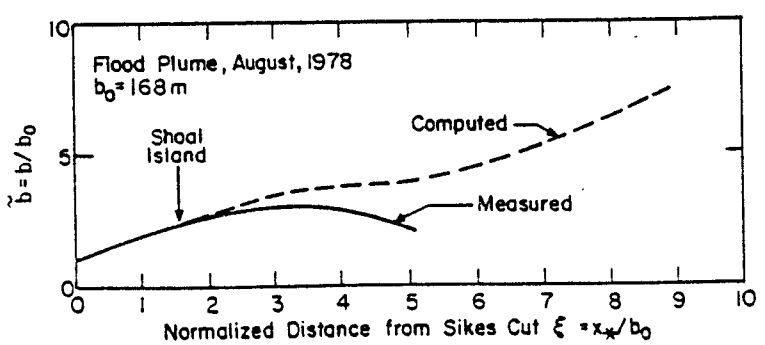

Fig. 10 Flood Plume Width Distribution, August 1978

Measured and computed boundary widths are compared in Fig. 10. After an initial agreement, the plume contracted more than what is predicted, beyond $\xi = 1.6$. This corresponds to the approximate location of the shoal island, which prevented the western boundary of the plume from expanding freely. Some effect of the shoal is also observed in Fig. 11 which shows the plume deflection. Between $\xi = 2$ and 5, the deflection is more than predicted. The $\theta = 78°$ limit occurred at $\xi = 7$, beyond which $\Omega = 0$ and $u_a = 0$ have been assumed. In spite of this approximation, there appears to be a reasonable agreement between the measured and the computed deflection, which is likely to be fortuitous to a degree. Also, inasmuch as $u_a = 0.01$ m/sec was measured at $\xi = 5.8$, its value up to the farthest extent of measurement, i.e. $\xi = 9$, was unknown. This renders any attempt to explain the observed agreement between measurement and prediction in the segment from $\xi = 7$ and $\xi = 9$ somewhat speculative.

In the above computations, the value of 0.031 m for k_s was used. In general, solutions of plume characteristics are somewhat sensitive to the magnitude of k_s. The effect of the variation in k_s was analyzed by utilizing the plume width and curvature data based on Fig. 7, which shows the plume in May, 1978. Even though the plume is incipient, it is possible to measure the width and curvature up to $\xi = 5$. It is observed in Fig. 12 that k_s must be increased from 0.031 m to 0.46 m, i.e. by a factor of 15, to predict the measured width. Fig. 13 shows the corresponding deflection. In the computations, $u_a = 0$ m/sec was assumed. The measured deflection agrees with the prediction between $\xi = 4$ and $\xi = 5$, but up to $\xi = 4$, the prediction somewhat underestimates the deflection. It should be mentioned that $k_s = 0.48$ m is of the same order as $k_s = 0.29$ m in the inlet. Furthermore, the effect of a 15-fold increase in k_s produces a much smaller change in the friction factor f and, therefore, in the bottom shear stress, according to Eq. 12. Thus for example selecting $H = 1$ and $h_o = 3$ m, f increases from 0.025 to 0.063, i.e. a less than 3-fold increase.

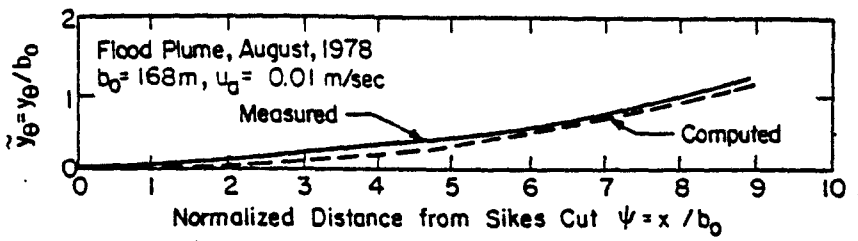

Fig. 11 Flood Plume Deflection, August 1978

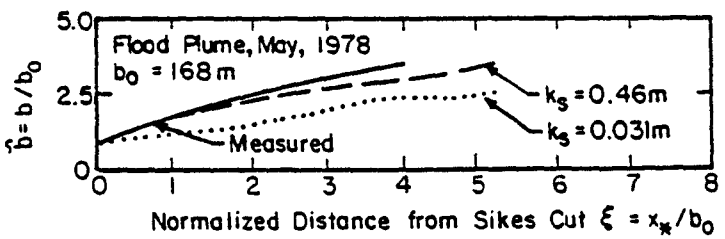

Fig. 12 Flood Plume Width Distribution, May 1978

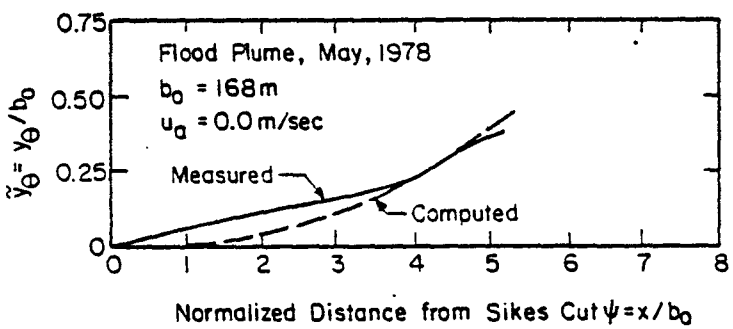

Fig. 13 Flood Plume Deflection, May 1978

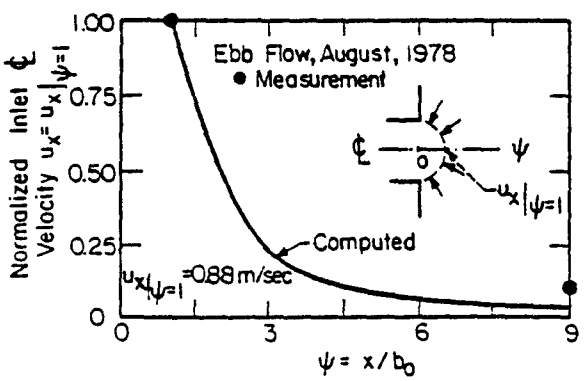

Fig. 14 Ebb Flow Inlet Centerline Velocity, August 1978

Ebb Flow

Ebb flow data were limited due to malfunctioning of some current meters; hence, only a minimal amount of comparison with prediction was possible. Eqs. 17, 20 and 21 were utilized with $P_t = 6.1 \times 10^6$ m^3, n = 6 and $\theta_e = \pi/6$. In the bottom topography of Fig. 5, the depth h(x) was converted to h(r) by simple transformation. In Fig. 14 the distribution of velocity $u_r = u_x$ along the inlet centerline is shown. Comparison with prediction based on measurements at ψ = 1 and 9 at least suggests an order of megnitude agreement.

Area of Influence of Sikes Cut

The maximum influence of the inlet in the bay may be expected to occur during spring tide. Selecting $P_t = 6.1 \times 10^6$ m^3 as the spring tidal prism, Eqs. 13 through 16 were solved to yield x_{*m} = 2,150 m as the longitudinal extent of influence of the inlet during flood. The value of k_s = 0.031 m was used for roughness in determining the plume characteristics since, a lower value of k_s causes the plume to expand less; hence for a given tidal prism, the plume penetration is greater.

In Fig. 15, the boundaries of the flood and the ebb flow distributions have been sketched. In an attempt to obtain a somewhat more realistic view of the plume, a frontal cap has been drawn (dash line). This has been done in a qualitative manner, by giving consideration to the following, namely: 1) the observation based on other inlets that the cap may be approximated by a semi-circle, 2) the scaling of the cap radius based on satellite images of the Sikes Cut plume on the Gulf side and 3) the continuity of mass in choosing the position of the cap center (Zeh, 1979; Mehta and Zeh, 1979). It is observed that the flow pattern influenced by the inlet is fairly localized, and that the existing reefs appear to be distant from the influence of this inlet. It can of course be argued that it is possible that the reef predators, once they enter the bay, remain there and cause a continued damage. Nevertheless, this possibility also exists with respect to the

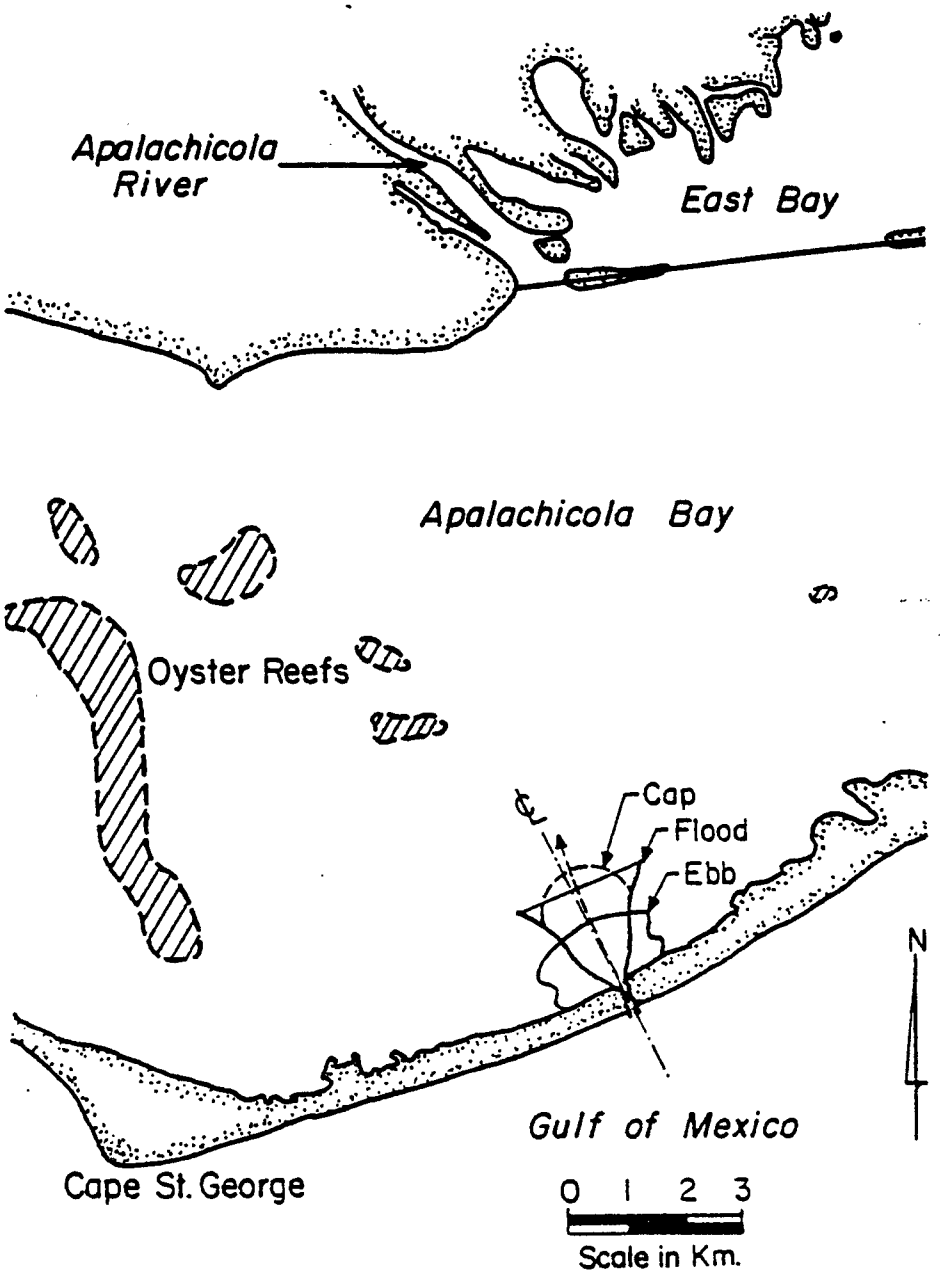

Fig. 15 Extent of Influence of the Inlet in the Bay

other openings, all of which indeed are much larger than Sikes Cut, and therefore such an argument does not appear to be sufficiently tenable in pointing to any influential role of Sikes Cut with respect to the reefs.

It appears that other expalanations must be sought as causative factors in oyster reef degradation. One is the construction of a dam for generating hydro-electric power upstream on Apalachicola River. This dam has reduced the peak value of the freshwater discharge in the river, resulting in an increase in the salinity throughout the bay (Boynton, 1975). Oyster reefs are in general sensitive to salinity changes and are conceivably affected adversely in a comparatively high saline environment.

SUMMARY AND CONCLUSIONS

The tidal influence of a small inlet, Sikes Cut, in the large and shallow Apalachicola Bay has been investigated. This bay, which produces nearly ninety percent of oysters in Florida, is connected to the Gulf of Mexico through several inlets, the smallest of which is Sikes Cut. Concern was expressed by the oyster industry that since the opening of this inlet in 1954, its presence has been responsible for the degradation of some of the oyster reefs in the vicinity.

The flood flow issuing from the inlet is modeled as a non-buoyant jet, whereas the ebb flow is approximated by considering the inlet to be a flow sink. These flow distributions have been verified with the help of measurements near the inlet. The maximum influence of the inlet in the bay is then estimated by considering the aerial extent of the flood and the ebb flow distributions at spring tide. Comparing these with the existing oyster reef locations tends to suggest that the influence of the inlet flow on these reefs is likely to be minimal. It is therefore suggested that some other factor such as the rise in salinity in the bay due to the construction of a dam on Apalachicola River is possibly the cause of the oyster reef degradation.

ACKNOWLEDGEMENT

Funds for this study were made available by State University System of Florida Sea Grant, NOAA, U.S. Department of Commerce, project number R/OE-10.

REFERENCES

Boynton, W.R., 1975. Energy Basis of a Coastal Region: Franklin County and Apalachicola Bay, Florida. Ph.D. Dissertation, Univ. of Florida, Gainesville, Florida.

Daily, J.W. and Harleman, D.R.F., 1966. Fluid Dynamics. Addison-Wesley, Reading, Massachusetts.

French, J.L., 1960. Tidal Flow in Entrances. U.S. Army Corps of Engineers Committee on Tidal Hydraulics, Tech. Bull. No. 3, Waterways Experiment Station, Vicksburg, Mississippi.

Hamming, R.W., 1968. Numerical Methods for Scientists and Engineers. 2nd Ed., McGraw-Hill, New York.

Mehta, A.J. and Zeh, T.A., 1979. Investigation of the Hydrodynamics of Inlet Plume. Proceedings of Specialty Conf. on Conservation and Utilization of Water and Energy Resources, ASCE, San Francisco, pp. 478-485.

Özsoy, E., 1977. Flow and Mass Transport in the Vicinity of Inlets. Coastal and Oceanographic Eng. Lab. Tech. Rept. No. 36, University of Florida, Gainesville, Florida.

Stolzenbach, K.D. and Harleman, D.R.F., 1971. An Analytical and Experimental Investigation of Surface Discharges of Heated Water. Ralph M. Parsons Lab. for Water Resources and Hydrodynamics, Rept. No. 135, M.I.T., Cambridge, Massachusetts.

Taylor, R.B., and Dean, R.G., 1974. Exchange Characteristics of Tidal Inlets. Proc. Coastal Eng. Conf., 14th, Copenhagen, Denmark, ASCE, 3, pp. 2268-2289.

Ünlüata, Ü.A. and Özsoy, E., 1977. Tidal Jet Flows Near Inlets. Proc. Hydr. in the Coastal Zone, ASCE, pp. 90-96.

Zeh, T.A., 1979. An Investigation of the Flow Field Near a Tidal Inlet. M.S. Thesis, Univ. of Florida, Gainesville, Florida.

LIST OF FIGURES